environments

MDPI

Article

Characterisation of Atmospheric Microplastics in Dry and Wet Deposition Using Size Fractionation and Raman Spectroscopy in Porto, Portugal

Yuliya Logvina [1], Rui Vilarinho [2], J. Agostinho Moreira [2], Helena Ribeiro [3], Luís Pinto da Silva [1] and Joaquim Esteves da Silva [1,*]

[1] Chemistry Research Unit (CIQUP), Institute of Molecular Sciences (IMS)—DGAOT, Faculty of Sciences of University of Porto (FCUP), Rua do Campo Alegre 697, 4169-007 Porto, Portugal; up201407073@edu.fc.up.pt (Y.L.); luis.silva@fc.up.pt (L.P.d.S.)
[2] IFIMUP, Departamento de Física e Astronomia, Faculdade de Ciências da Universidade do Porto, Rua do Campo Alegre s/n, 4169-007 Porto, Portugal; rvsilva@fc.up.pt (R.V.); jamoreir@fc.up.pt (J.A.M.)
[3] Department of Geosciences, Environment and Spatial Plannings (DGAOT), Earth Sciences Institute (ICT), Faculty of Sciences of University of Porto (FCUP), Rua do Campo Alegre 697, 4169-007 Porto, Portugal; helena.ribeiro@fc.up.pt
* Correspondence: jcsilva@fc.up.pt

Abstract

The characterisation of airborne microplastics (MPs) and synthetic fibres in Porto, Portugal, is presented alongside an evaluation of how rainfall influences their abundance, composition, and size distribution. Six atmospheric samples (three dry-deposition and three wet-deposition) were collected in an urban residential area of Porto using a Microplastic NILU collector. Samples were subjected to a size-fractionation filtration procedure that separated particles into environmentally relevant size classes (5 mm–125 μm, 125–63 μm, 63–25 μm, 25–12 μm, and 12–1.2 μm), with each size class retained on cellulose nitrate membranes. This preparation enabled targeted morphological and chemical analyses while reducing particle overlap and improving detection efficiency. The fractionated samples on filters were subsequently analysed using optical microscopy, scanning electron microscopy (SEM), and micro-Raman spectroscopy to ensure robust identification and morphological assessment. Wet deposition, based on optical microscopy quantification, showed substantially higher deposition rates, exhibiting approximately 8.5 times higher MP accumulation and nearly 3 times higher fibre accumulation than dry deposition: the dry-deposition mean was 427 MPs d^{-1} m^{-2} (SD = 190), 2305 fibres d^{-1} m^{-2} (SD = 829), and the wet-deposition mean was 3629 MPs d^{-1} m^{-2} (SD = 449), 6515 fibres d^{-1} m^{-2} (SD = 2683). Blue was the predominant colour for both MPs fragments and fibres. Raman characterisation of a selected subset (Category I) of visually suspected MPs and fibres showed that acryl (PMMA) was the dominant polymer in both conditions, followed by polyester (PES) and polypropylene (PP). A high abundance (up to ~109,000 extrapolated particles) of brightly coloured, unnatural-looking submicron particles, below the Raman detection threshold, was identified by optical microscopy in two wet-deposition samples but not in dry samples. The findings highlight the importance of integrating particle morphology, size fractionation, polymer composition and deposition mode when characterising atmospheric MPs and fibres.

Keywords: microplastics; fibres; atmosphere; aerosols; Raman identification; microplastics size fractionation

Academic Editor: Ana Luísa Patrício da Silva

Received: 21 October 2026
Revised: 14 November 2026
Accepted: 20 November 2026
Published: 25 November 2026

Copyright: © 2026 by the authors. Licensee MDPI, Basel, Switzerland. This article is an open access article distributed under the terms and conditions of the Creative Commons Attribution (CC BY) license.

1. Introduction

Microplastics (MPs) are persistent environmental contaminants that can be transported between environmental compartments. Although their occurrence has been extensively investigated in marine, freshwater and terrestrial environments, the atmosphere has received comparatively less attention. Airborne MPs can be transported over considerable distances and subsequently transferred to terrestrial and aquatic environments through dry and wet deposition. Their atmospheric occurrence, sources, transport pathways and deposition processes therefore remain important areas of investigation [1–7].

Atmospheric MPs originate from multiple anthropogenic sources, including textile fibres, traffic-related emissions, tyre wear, and the resuspension of contaminated road dust, soils, and other environmental surfaces [8–13]. These sources produce particles with different physical and chemical characteristics, contributing to substantial variability in atmospheric MP abundance and composition. Among the particle morphologies commonly reported, fibres and fragments are particularly important [14]. Their different shapes and aspect ratios can influence atmospheric transport, deposition behaviour and analytical recovery, making morphology an important consideration when characterising airborne MPs [14–17].

Despite increasing interest in atmospheric MPs, comparisons among studies remain difficult because sampling and analytical procedures vary considerably [18]. Differences in collection devices, size-fractionation strategies, filter materials and identification techniques can influence the particles recovered and subsequently characterised [18,19]. In particular, the separation of particles according to size and morphology, together with reliable chemical identification, is necessary to distinguish synthetic polymers from natural and other atmospheric particles [8,14–17,20]. Raman spectroscopy provides an important tool for polymer identification, but atmospheric ageing, fluorescence, pigments, additives and weak spectral signals can limit the identification of individual particles [18,21].

An additional challenge is the characterisation of particles associated with atmospheric deposition under different meteorological conditions. Dry and wet deposition represent distinct pathways for the transfer of airborne particles to the surface, and rainfall may modify both the quantity and characteristics of particles removed from the atmosphere [6,7]. However, comparisons of dry and wet deposition that simultaneously consider particle abundance, morphology, size fraction and polymer composition are not always evaluated together within the same sampling and analytical framework [18]. A methodology integrating these characteristics can therefore provide a more complete description of atmospheric MP deposition than particle counts alone.

The distinction between fibres and other microplastic morphologies is also relevant in the context of the European Chemicals Agency (ECHA) definition under the REACH Regulation (Commission Regulation (EU) 2023/2055, Annex XVII, Entry 78). According to this regulatory definition, fibre-like synthetic polymer microparticles are characterised by a length equal to or below 15 mm and a length-to-diameter ratio greater than 3, whereas non-fibrous particles are defined by a maximum dimension of 5 mm. However, morphological characteristics alone are insufficient to establish whether a fibre is synthetic, since atmospheric fibres may originate from both natural and synthetic materials.

In this context, the present study applies a size-fractionated passive sampling approach, combined with optical microscopy, SEM, and micro-Raman spectroscopy, to characterise MPs and fibres collected during dry and wet atmospheric deposition in Porto, Portugal. The approach enables evaluation of particles across five size fractions, from 5 mm to 1.2 μm, while accounting for their morphology and polymer composition. Raman spectra were further classified by the degree of polymer identification, enabling examina-

tion of how particle characteristics and deposition conditions influence chemical identification. The passive sampling approach used here builds on the methodology developed in our previous studies [19,22].

The methodological contribution of this study is the integration of deposition mode, particle morphology, size fraction and polymer composition within a single sampling and analytical framework. This approach allows dry and wet atmospheric deposition to be compared not only in terms of particle abundance but also in the types of particles recovered and the reliability of their chemical identification.

Accordingly, the objectives of this study were to (i) compare the abundance of MPs and fibres in dry and wet atmospheric deposition; (ii) evaluate their distribution across size fractions and morphological characteristics; (iii) characterise their polymer composition using micro-Raman spectroscopy; and (iv) assess how deposition conditions and sample processing influence particle recovery and polymer identification.

2. Materials and Methods

2.1. Sampling Site and Atmospheric Deposition Collection

Six atmospheric MP samples were collected in Porto, the second-largest city in Portugal. The dataset comprises three dry-deposition samples (A1–A3) and three wet-deposition samples (B1–B3) collected during June–July 2024. Dry deposition samples were collected cumulatively over 8-day periods (A1: 3–11 June; A2: 1–9 July; A3: 22–30 July), representing particle deposition under dry atmospheric conditions. Wet deposition samples were collected over 24 h periods during rainfall events (B1: 11–12 June; B2: 9–10 July; B3: 30–31 July) on the day following after each dry cumulative sampling period, representing particles scavenged from the atmosphere by precipitation (Figure 1).

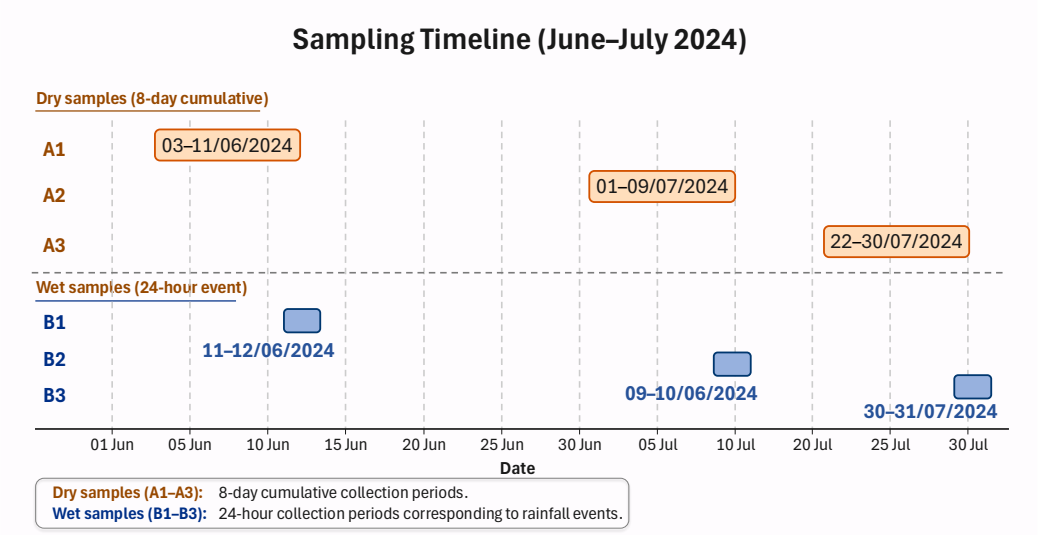

Figure 1. Sampling chronology of dry- and wet-deposition sample collection.

Passive sampling procedures previously described in the study were followed [22]. The collection was carried out using a NILU Innovation Microplastic Collector, designed in accordance with the draft ISO 4222.2 [23] standard for particulate deposition collectors. The device minimised cross-contamination and was positioned at the Faculty of Sciences, University of Porto (41.151629, −8.637068), 2.30 m above ground level, at the exact location as in earlier campaigns [22]. The sampling site is located in an urban residential area with heavy road traffic and close to a major city entrance. Additional sample-level information,

including the collector type, effective collection area, sampling height and GPS coordinates, together with the collection dates and sampling durations, is provided in Table S3 (Supplementary Material).

2.2. Sample Processing and Size Fractionation

After collection, the samples were transferred from the collector to a dark glass vial using deionised water and a stainless steel funnel with a 5 mm mesh, as shown in Figure 2. The samples were stored at 4 °C until processing.

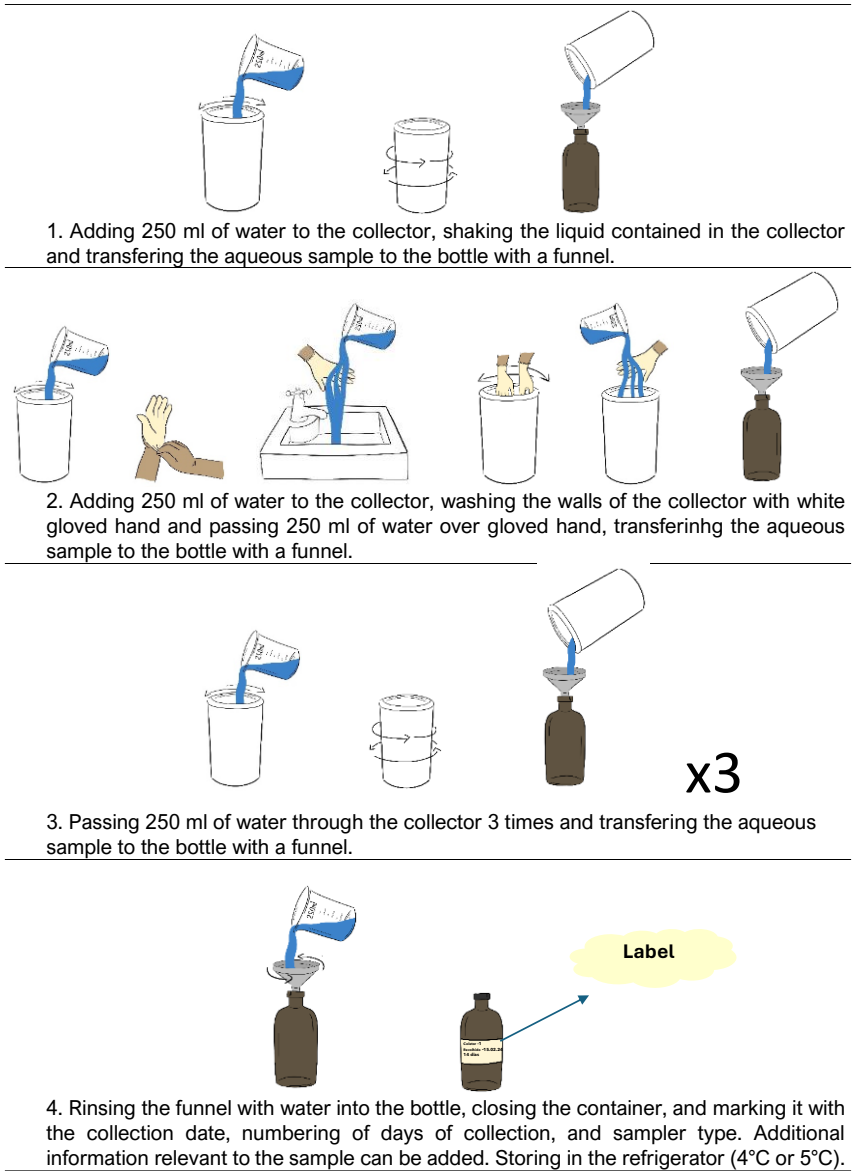

Figure 2. Schematic representation of sample transfer from the collector to a dark glass vial using deionised water and a stainless steel funnel with a 5 mm mesh.

The equipment and procedures used for sample processing were consistent with those described in previous studies [22]. In brief, a vacuum pump (KNF LABOPORT No. 96, Schenkon, Switzerland) was used to pass the samples through stainless steel sieves (HAVER & BOECKER, Oelde, Germany) with mesh pore sizes of 125 µm, 63 µm, and 25 µm, followed by filtration through a glass filtration vacuum system (Normax, Marinha Grande, Portugal) equipped with cellulose nitrate (CN) membrane filters (Whatman® Cytiva, Maidstone, UK) with pore sizes of 12 µm and 1.2 µm for size fractionation of the

aqueous samples (direct filtration). A sonicator (VWR Ultrasonic Cleaner, Radnor, PA, USA) was used to disperse the aggregates. An oven (Heraeus Instruments, Hanau, Germany) was used to digest the mesh-retained organic matter with 15% hydrogen peroxide (H_2O_2, Carlo Erba Reagents—DasitGroup, Cornaredo, Italy) at 50 °C for 12 h, followed by refiltration of the particulate matter, again using meshes (pore-sizes of 125 µm, 63 µm, and 25 µm) and CN membrane filters (12 µm and 1.2 µm). The workflow is presented in Figure S1 of the Supplementary Material.

Overall, samples were separated into five size fractions (5 mm–125 µm; 125–63 µm; 63–25 µm; 25–12 µm; and 12–1.2 µm). For the two smallest fractions (25–12 µm and 12–1.2 µm), results were obtained from both direct filtration and from oxidative digestion of material retained in the larger fractions, thereby allowing particles associated with organic matter or aggregates to be recovered. The post-digestion counts therefore represent coarse particles and recovered additional particles of fine fractions. Fine particles recovered through direct filtration, and those recovered following H_2O_2 digestion of the material retained on the larger meshes were counted separately.

2.3. Quality Assurance/Quality Control

To minimise potential contamination during sample processing, glass and stainless steel equipment was used wherever possible, and procedural blanks were prepared using deionised water and subjected to the same filtration procedure as the samples. Blank results were evaluated for each size fraction and subtracted from the corresponding sample values. Blank filters were also analysed by µ-Raman spectroscopy to assess potential spectral contributions from the filtration materials and background particulate matter. The equipment and sample-processing procedures followed those described in our previous study [22].

2.4. Microscopy and Morphological Characterisation

After processing, membrane filters were stored in Petri dishes until analysis. Particles were initially examined using optical microscopy (VisiScope® 534, VWR®, Radnor, PA, USA) with 10×, 20× and 40× objectives. Particle abundance, morphology and colour were recorded for each size fraction.

Particle identification by optical microscopy was based on morphological characteristics and visual appearance. Bright, unnaturally coloured fragments displaying colours commonly associated with manufactured materials (red, blue, green, yellow, orange and purple/pink) were initially classified as visually suspected MPs. Fibres were recorded separately and classified as transparent, blue or other coloured fibres (Table S1, Supplementary Material). However, optical microscopy alone cannot confirm their polymeric composition. Therefore, this classification represents a preliminary morphological assessment.

To confirm polymer composition, representative particles were subsequently characterised using SEM and µ-Raman spectroscopy. SEM analysis was performed using an FEI Quanta 400 ESEM equipped with an EDAX Genesis X4M system at 15.0 kV without conductive coating. Selected regions of the CN membrane filters were examined after mounting on carbon tape. Particles with distinctive morphological characteristics were selected for SEM examination.

2.5. Raman Spectroscopic Analysis and Polymer Classification

Raman analysis was performed using an inVia™ Renishaw micro-Raman spectrometer over the spectral range 200–3200 cm^{-1}, with a spectral resolution of 1 cm^{-1}. Raman analysis was performed on a selected subset of particles from all samples and across the five size fractions. Particle selection was not proportional to the total abundance of fibres

and MPs recorded by optical microscopy. This was primarily based on practical constraints, including schedule limitations, spectral acquisition time, and access to the equipment. Therefore, an approximate target of 300 MP fragments and spherical particles per deposition mode was adopted. In total, 292 MP fragments and 27 spheres were analysed in dry deposition, compared with 299 MP fragments and 18 spheres in wet deposition. Considering spheres within the MP category, these numbers correspond to approximately 80.2% and 78.9% of the optically recorded MP counts in dry and wet deposition, respectively. Due to their substantially higher abundance, fibres were analysed as a smaller subset, comprising 243 fibres in dry deposition (12.5% of the optically recorded fibres) and 303 fibres in wet deposition (35.5%). The analysed particles covered all five size fractions and included different colours and particle morphologies (see Table S2, Supplementary Material).

A 50× objective was used for particle analysis, with excitation wavelengths of 785 or 532 nm (0.02–2 mW) selected according to particle characteristics and spectral response. To minimise analysis time while maintaining spectral quality, spectra were acquired using a single 15s acquisition. Spectra were processed using Savitzky–Golay smoothing (third-order polynomial, with a 15-point window), intelligent-fit baseline correction (noise factor 1.5; polynomial order 11) and normalisation to a constant integrated area of 1, based on a critical review of processing and classification techniques for images and spectra in microplastic research [24].

To evaluate potential contributions from the filter membrane and background particulate matter, each membrane was additionally analysed at three points along the filter edge and three randomly selected particle-free areas of the membrane using the 50× objective.

Raman spectra were compared with the open SLoPP and SLoPP-E spectral databases for polymer identification and with the CHSOS pigment database for pigment assignment [21,25]. Polymer assignments were based on the agreement of multiple diagnostic Raman bands and the consistency of the overall spectral profile with the corresponding reference spectra, rather than on individual peak matches alone. Particular attention was given to the presence, relative intensities and positions of characteristic bands, while considering potential spectral contributions from pigments, additives and other interfering materials.

Spectra with diagnostic bands allowing unequivocal polymer identification were assigned to Category I: Unambiguously Identified Polymers. Where the spectral characteristics supported assignment to a polymer family but did not allow discrimination among closely related polymers, particles were assigned to Category II: Polymers Grouped into Chemically Similar Families. The families considered were styrene-based, polyester-type, polyamide-type, polyurethane-type, polyolefins, nitrogen-containing, acrylic-type and vinyl-based polymers. Spectra dominated by fluorescence, pigment/additive signals, weak Raman response or insufficient spectral information were assigned to Category III: Indeterminate Synthetic Polymers.

2.6. Data Processing and Statistical Analysis

The reported deposition rates were calculated from particle counts obtained through optical microscopy. Therefore, they represent visually suspected MPs and visually identified fibres based on their morphological and visual characteristics. Raman analysis was performed on selected subsets of the optically identified particles, with different proportions analysed for MPs and fibres (Section 2.5), to characterise their chemical composition. The Raman results were not extrapolated to estimate the total particle abundance, and no Raman-based correction or spectroscopic confirmation factor was applied to the optical microscopy counts used to calculate deposition rates.

Deposition rates were calculated by dividing the number of MPs or fibres collected by the collector area and the corresponding sampling duration. Dry-deposition samples

collected over 8-day periods were therefore expressed as daily deposition rates (MPs d^{-1} m^{-2} and fibres d^{-1} m^{-2}), while wet-deposition samples collected over 24-hour periods were expressed on the same daily basis.

Descriptive statistics were calculated for each deposition mode and size fraction. Differences in MP and fibre deposition between dry and wet samples were evaluated using an exact Mann–Whitney U test. Because only three independent sampling events were available for each deposition mode (n = 3 per group), statistical comparisons were interpreted cautiously and considered exploratory. A significance threshold of $p < 0.05$ was used.

Data processing and statistical analysis were performed using Microsoft Excel (Microsoft 365 MSO, Version 2507, Build 16.0.19029.20136) and Origin 9.0. Hierarchical cluster analysis (HCA) was performed to evaluate similarities in polymer identification profiles based on their Raman-identified polymer composition. Euclidean distance was used to calculate dissimilarity between samples, and the resulting clusters were examined to assess whether samples clustered by deposition mode and/or polymer composition.

3. Results

3.1. Overall Deposition of MPs and Fibres

The total deposition rates of visually suspected MPs and fibres, as quantified by optical microscopy and calculated across all size fractions, differed markedly between dry- and wet-deposition samples (see Figure 3). Dry-deposition samples showed fibre deposition rates ranging from 1452 to 3108 fibres d^{-1} m^{-2}, with a mean of 2305 ± 829 fibres d^{-1} m^{-2}. MP deposition rates ranged from 294 to 645 MPs d^{-1} m^{-2}, with a mean of 427 ± 190 MPs d^{-1} m^{-2}. Wet-deposition samples showed higher deposition rates, with fibre values ranging from 4456 to 9549 fibres d^{-1} m^{-2} (mean 6515 ± 2683 fibres d^{-1} m^{-2}) and MP values ranging from 3215 to 4106 MPs d^{-1} m^{-2} (mean 3629 ± 449 MPs d^{-1} m^{-2}). Thus, the mean wet-deposition rate was approximately 2.8 times higher for fibres and 8.5 times higher for MPs than the corresponding dry-deposition rates. However, in dry samples, the fibre deposition rate was about 5 times higher than the MP deposition rate. In contrast, the number of fibres in wet-deposition samples ranged more widely, indicating greater variability among rainfall-associated sampling events.

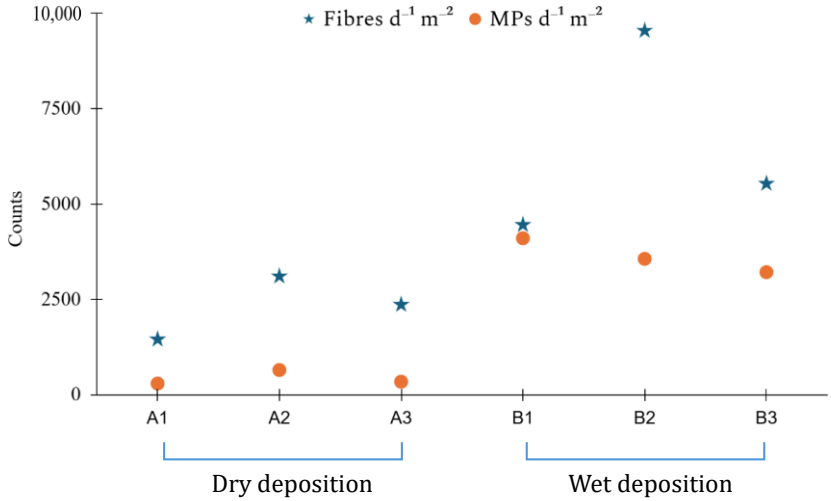

Figure 3. Comparing MPs and fibre counts, based on optical microscopy, per day and per square meter (MPs d^{-1} m^{-2}; Fibres d^{-1} m^{-2}) in the dry- and wet-deposition samples.

The exact Mann–Whitney U test gave U = 0 and p = 0.10 for both MP and fibre deposition rates. Therefore, despite the pronounced difference in the observed deposition rates,

the comparison did not reach the conventional significance threshold, and the results should be interpreted as descriptive evidence given the small number of independent sampling events (n = 3 per deposition mode).

3.2. Size Distribution and Effect of H_2O_2 Digestion

The distribution of visually suspected MPs and identified fibres by optical microscopy across the five size fractions showed distinct differences between dry- and wet-deposition samples (see Figures 4–6). Wet deposition generally showed higher abundances than dry deposition, particularly in the larger fibre fractions and in the fine MP fractions.

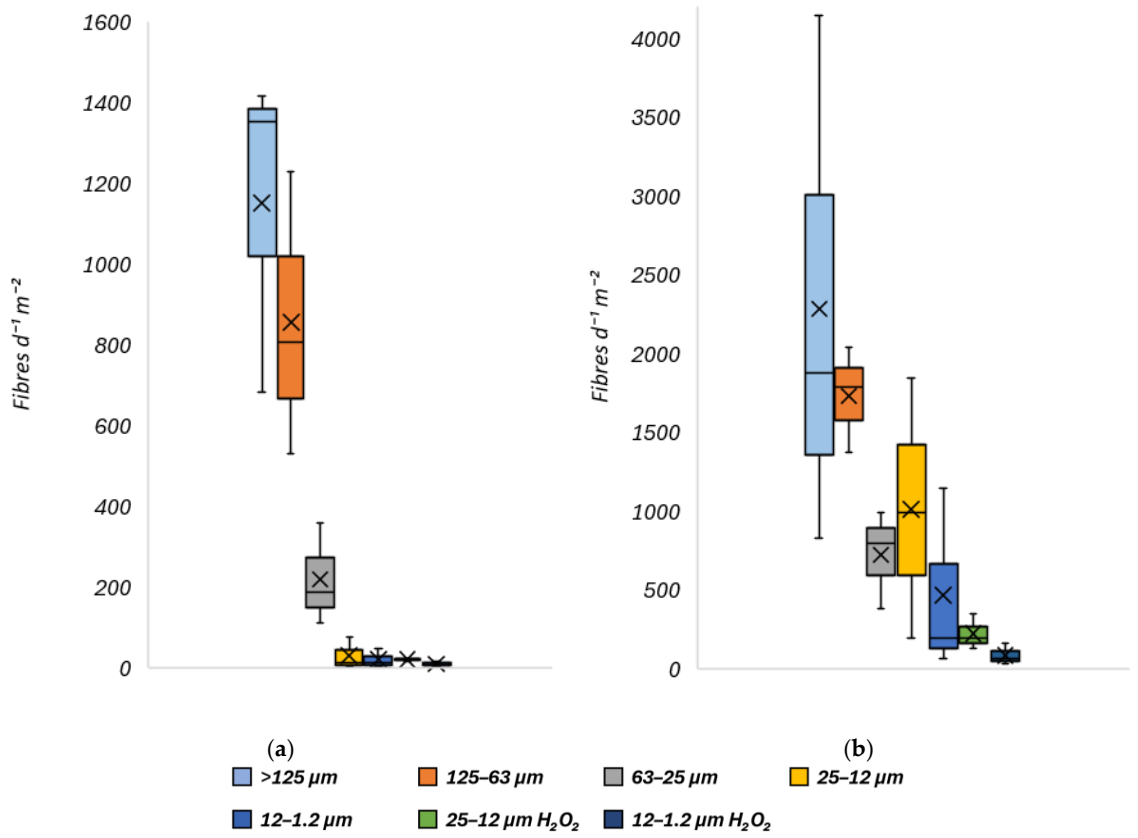

Figure 4. Box-plot distributions of fibre counts (Fibres d^{-1} m^{-2}) based on optical microscopy across size fractions for dry- and wet-deposition samples, with separate representation of H_2O_2-treated subsets of 25–12 µm and 12–1.2 µm fractions: (**a**) dry deposition, (**b**) wet deposition.

For fibres, the highest deposition rates occurred in the >125 µm and 125–63 µm fractions, whereas dry-deposition samples generally showed lower abundances and a decline towards the smaller fractions (see Figure 4). Wet-deposition samples also showed greater variability in the 25–12 µm and 12–1.2 µm fractions. MPs showed a similar overall pattern, with wet-deposition samples exhibiting higher values across most size fractions (see Figure 5). The 63–25 µm fraction showed the highest mean MP abundance and variability among wet samples, whereas dry-deposition samples showed lower and narrower distributions.

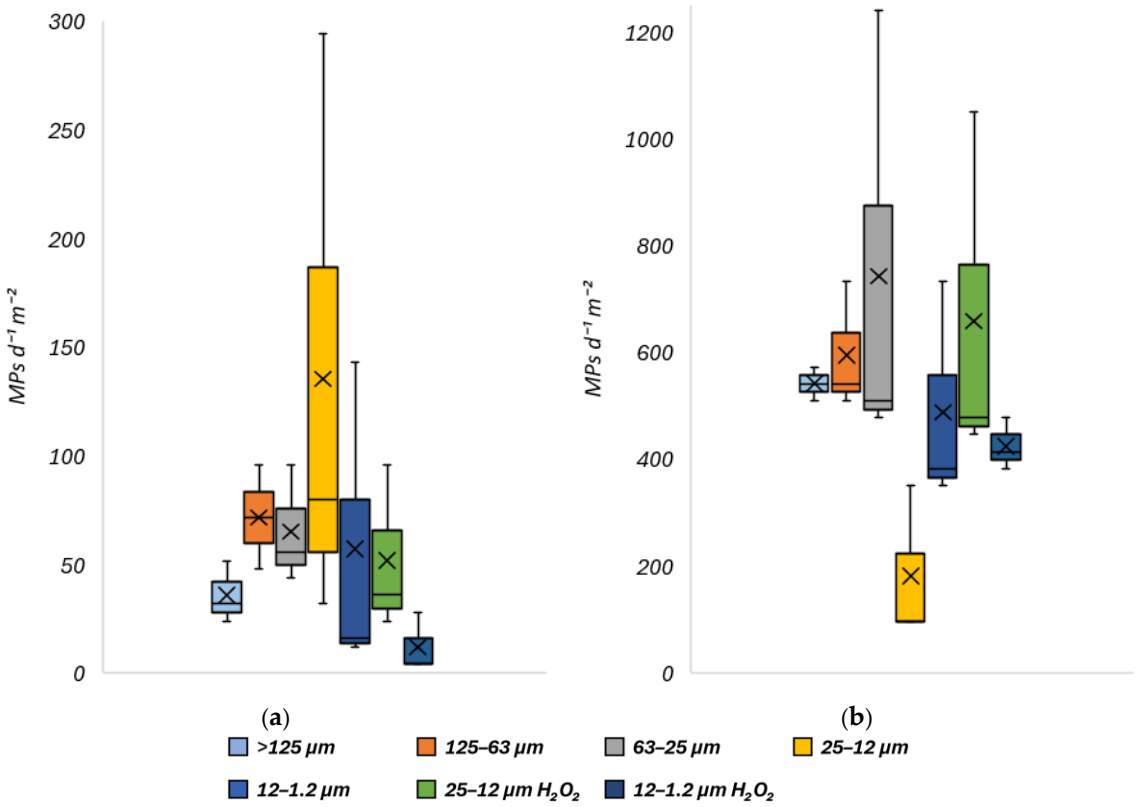

Figure 5. Box-plot distributions of microplastic counts (MPs d^{-1} m^{-2}) based on optical microscopy across size fractions for dry and wet samples, with separate representation of H_2O_2-treated subsets of 25–12 µm and 12–1.2 µm fractions: (**a**) dry deposition; (**b**) wet deposition.

Comparison of direct filtration with the material recovered after H_2O_2 digestion demonstrated that a proportion of visually suspected MPs in the fine fractions was associated with material retained in the larger fractions (see Figure 6). In dry deposition, 67.2% and 69.6% of MPs in the 25–12 µm and 12–1.2 µm fractions, respectively, were detected by direct filtration. In comparison, 32.8% and 30.4% were recovered after digestion. For fibres, 43.4% of particles in the 25–12 µm fraction and 61.1% in the 12–1.2 µm fraction were detected before digestion. In wet deposition, only 23.0% of MPs in the 25–12 µm fraction were detected by direct filtration, compared with 77.0% after digestion. In the 12–1.2 µm fraction, the corresponding proportions were 52.0% and 48.0%. Fibres showed the opposite pattern, with 75.9% and 72.0% detected before digestion in the 25–12 µm and 12–1.2 µm fractions, respectively. These results demonstrate that oxidative digestion substantially affected the recovery of fine MPs, particularly in wet-deposition samples.

Numerous submicron particles were observed in the 12–1.2 µm fraction of wet-deposition samples. These particles were below the Raman analytical size threshold (≤0.5 µm) and could therefore be detected visually but not chemically characterised. Magenta and yellow particles were abundant in wet sample B2, while deep-rose particles were observed in B3. Because of their high abundance, particle numbers were estimated by systematic subsampling. Each membrane filter was divided into nine counting areas distributed across the centre, intermediate and border regions, and the observed counts were extrapolated to the total filter area. The estimated abundance was approximately 85,000 magenta and 24,000 yellow particles in B2 (~109,000 particles in total), and approximately 51,000 deep-rose particles in B3. However, their polymeric nature could not be confirmed by Raman spectroscopy, and these extrapolated estimate values were not included in the reported visually suspected MP deposition rates, which were based exclusively on direct enumeration.

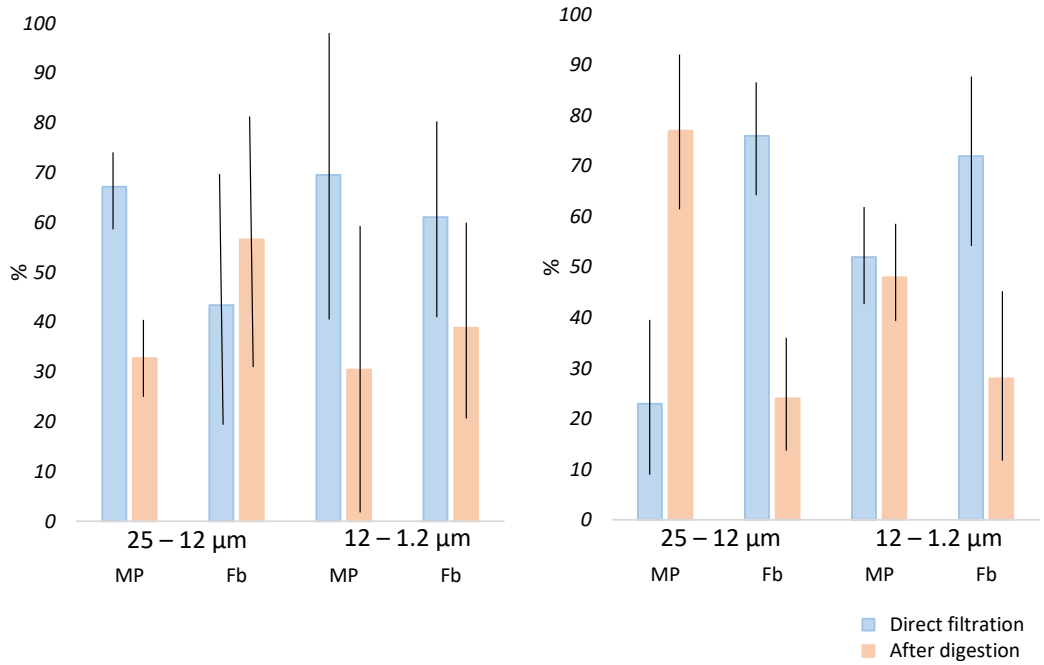

Figure 6. Effect of H_2O_2 digestion on MP and fibres in atmospheric samples, subsets of size fractions 25–12 µm and 12–1.2 µm, mean % values: (**a**) dry deposition; (**b**) wet deposition. MP: microplastics; Fb: fibres.

3.3. Morphological Characteristics of MPs and Fibres

Initial observations of membrane filters from five studied size fractions, under the optical microscope, showed that the majority of bright, unnaturally coloured fragments classified as suspected MPs were blue. Among the visually suspected MPs counted, 47.2% were identified as blue fragments in dry deposition and 61.8% in wet deposition, while the remaining were of other colours (see Figure 7). In fibres, results revealed that for dry-deposition samples, 12.5% of fibres were blue, 73.0% were transparent, and 14.5% fell into the "other" category. For wet-deposition samples, 37.8% of fibres were blue, 50.0% were transparent, and 12.1% the "other" category. These results indicate that when fibres and MPs are coloured, there is a clear predominance of blue MPs and fibres in the analysed samples.

The anisotropic geometry of the fibres posed clear challenges for the size-fractionation process. During sieving, fibres behaved differently from fragments: depending on their orientation, a fibre could pass vertically through a mesh opening but fail to pass when positioned horizontally. As a result, the distribution of fibres across size fractions was less consistent than that of fragments. Under optical microscopy, fibres also proved more difficult to quantify reliably. Their elongated and often curled shapes—sometimes forming compact clews—complicate detection and manual measurement, unlike the more regular and easily quantifiable geometries of fragments (see Figure 8). SEM images also showed fraying, cracking, and longitudinal splitting (see Figure 9).

Coloured spherical particles were observed in both deposition modes and across several size fractions (see Figure 10), with no particular prevalence of one sampling type over the other. They ranged from 1 to 6 MP spherical particle counts in the fraction and from 7 to 10 MP spherical particle counts by sample. Any single sphere was evident in the blank samples. In the quantification process, these spheres were included both within the corresponding colour categories of MPs and in a separate column explicitly dedicated to spheres (Table S1, Supplementary Material).

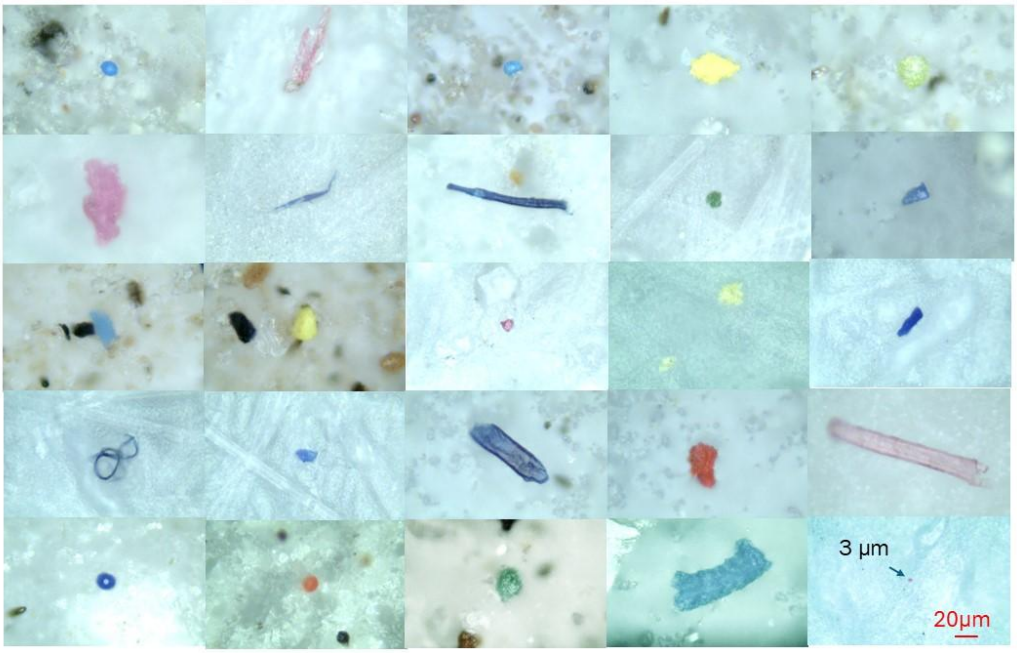

Figure 7. Representative optical microscope images of visually suspected MPs and fibres from dry- and wet-deposition samples.

Moreover, black and brown fragments were observed in both deposition modes, occurring as both spherical particles and irregular fragments. To verify whether these particles were associated with tyre-wear residues, they were analysed using Raman spectroscopy. Their spectra matched the soot reference spectra reported in the study [26].

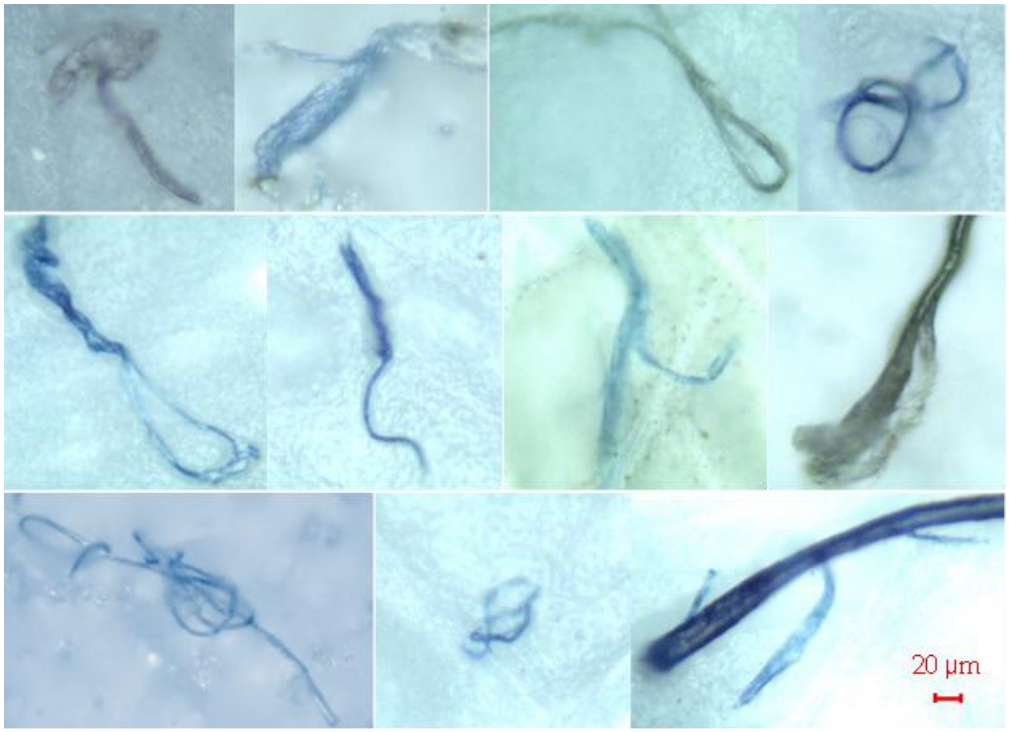

Figure 8. Representative optical microscope images of fibres from dry- and wet-deposition samples.

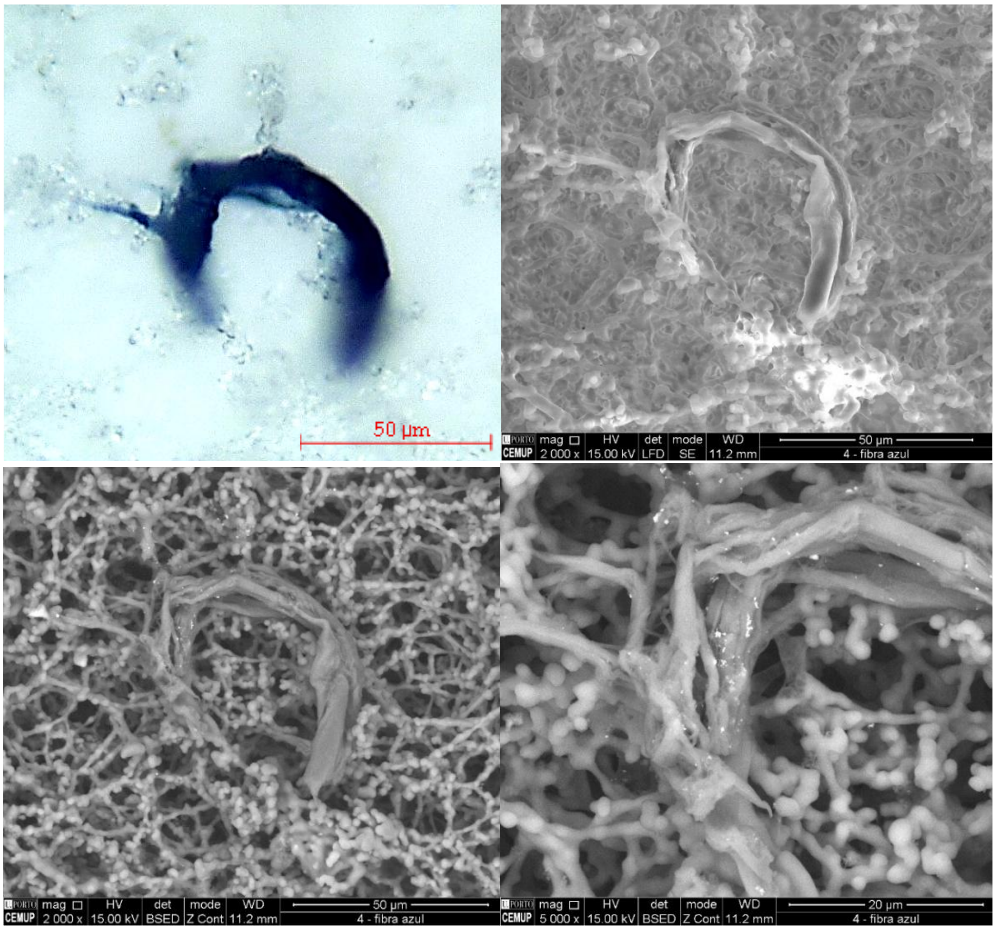

Figure 9. Optical microscope and SEM images of a blue fibre in the deposition samples.

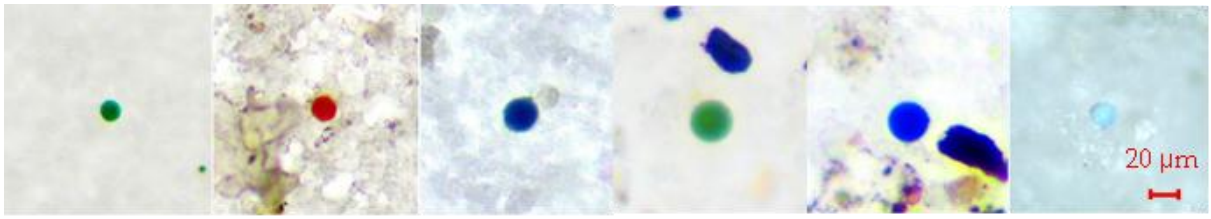

Figure 10. Representative optical microscope images of coloured spheres from dry- and wet-deposition samples.

3.4. Raman Identification and Polymer Composition

Raman spectroscopy was employed to characterise the chemical composition of selected particles identified through optical microscopy across all dry- and wet-deposition samples and size fractions. The selection strategy and the corresponding proportions of particles subjected to Raman analysis are described in Section 2.5. In total, 1182 Raman spectra were acquired, comprising 546 fibres, 591 MP fragments and 45 spheres (dry samples: 243 fibres, 292 MP fragments and 27 spheres; wet samples: 303 fibres, 299 MP fragments and 18 spheres) and presented in Table S2 (Supplementary Material). The analysis allowed the distinction between synthetic polymers, natural fibres, and other non-plastic particulates commonly present in atmospheric fallout. Scarce spherical particles were not reported as a separate category in this article and were instead included within the colour-coded microplastic categories in the analysis reports. Quantitative records of spherical particles are provided in Table S1 of the Supplementary Material.

Raman spectroscopy enabled polymer identification by comparing experimental spectra with reference spectra from the SLoPP and SLoPP-E databases. Some representative examples of Category I identification are presented in Figures 11–13. Figure 12 also illustrates potential spectral interference associated with an indigo-containing acrylic binder documented in the CHOS database. A residual band in the region of 1730 cm^{-1} remained detectable, consistent with the ester carbonyl stretching vibration characteristic of weathered PMMA, alongside other PMMA-compatible features in the fingerprint region (601 cm^{-1}—skeletal vibration; 1464 cm^{-1} CH_3 deformation). In contrast, no distinct nitrile stretching band around 2240 cm^{-1}, characteristic of PAN-based acrylic, was detected. These combined spectral features supported the PMMA assignment over PAN, although the reduced intensity of some bands and potential spectral interference were considered when evaluating the identification. To investigate potential spectral interference, the experimental spectrum was additionally compared with reference spectra of pure synthetic indigo and synthetic indigo mixed with acrylic binder, acquired at 785 nm. The comparison revealed overlap between the experimental spectrum and indigo-related bands, particularly in the regions around 550, 1229, 1316, 1465 and 1577 cm^{-1}. However, neither the pure indigo nor the acrylic binder references exhibited a clearly resolved band around 1730 cm^{-1}, corresponding to the characteristic ester carbonyl stretching vibration. This observation, together with the comparison with PMMA reference spectra, provided additional support for the PMMA assignment, while recognising the potential contribution of pigment-related signals to other spectral features.

A representative example of a spectrum assigned to Category II is shown in Figure S2, Supplementary Material. The spectrum exhibited a prominent peak at approximately 1000–1001 cm^{-1}, supporting its assignment to the styrene-based polymer family; however, identification of a specific polymer was not possible. Figure S3 (Supplementary Material) presents a comparison of the raw and processed Raman spectra classified as Category III (indeterminate synthetic polymer). Despite spectral processing, the spectrum did not provide sufficient diagnostic evidence to assign the particle to an individual polymer or a chemically similar polymer family. Figure S4 (Supplementary Material) illustrates a Category III spectrum for which the available spectral features were insufficient to establish a reliable polymer or polymer family assignment due to fluorescence obscuring picks.

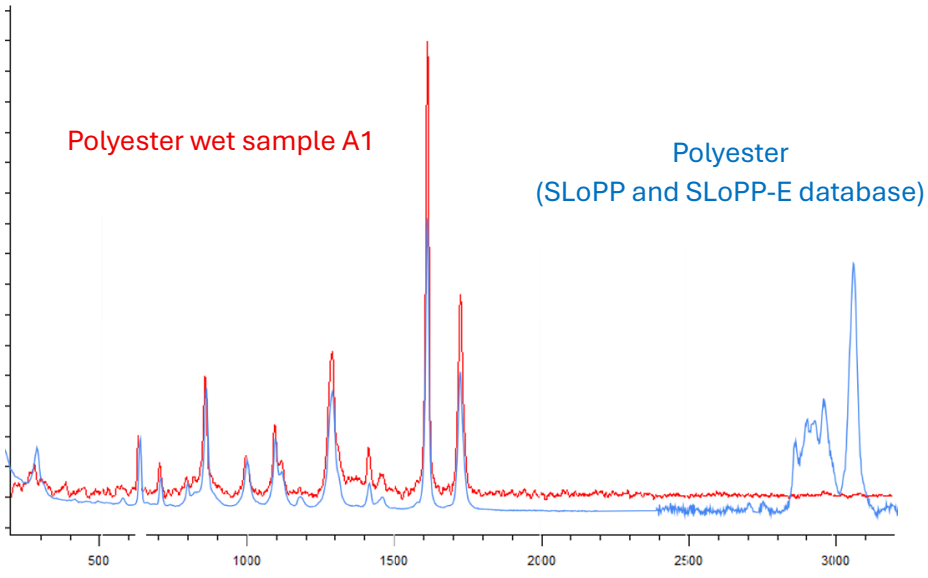

Figure 11. Raman spectral profile of a representative polyester particle identified in this study, alongside corresponding reference spectra from the SLoPP and SLoPP-E databases, classified as Category I.

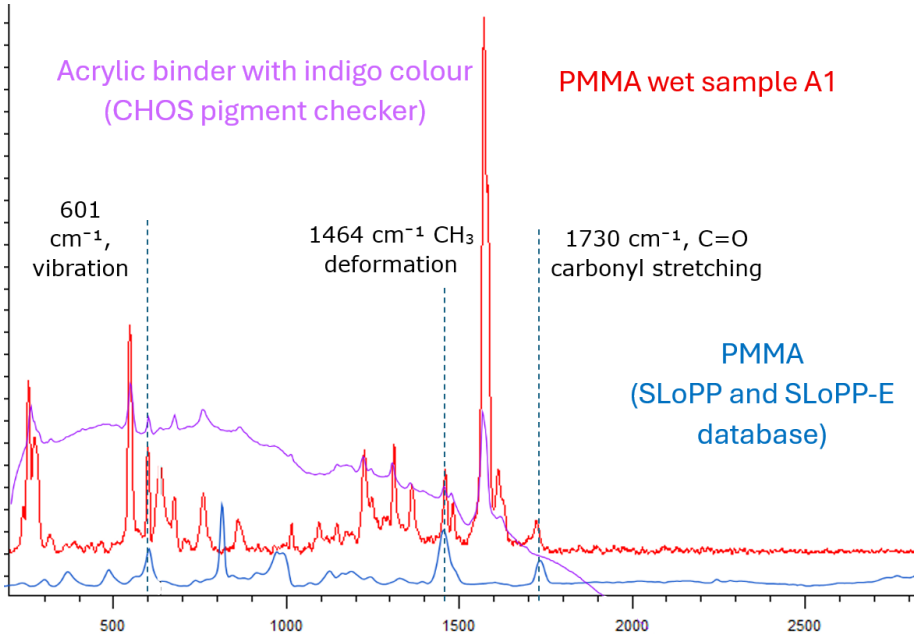

Figure 12. Raman spectral comparison supporting the assignment of a particle to poly(methyl methacrylate) (PMMA) (SLoPP and SLoPP-E database), highlighting potential spectral interference from an indigo-containing acrylic binder documented in the CHOS database, classified as Category I.

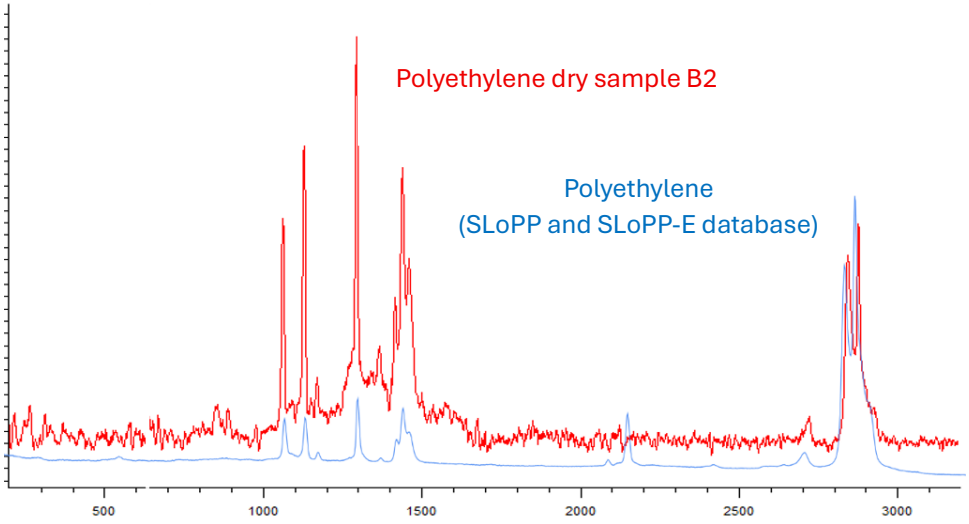

Figure 13. Raman spectral profile of a representative polyethylene particle identified in this study, alongside corresponding reference spectra from the SLoPP and SLoPP-E databases, classified as Category I.

Category I (unambiguously identified polymers) accounted for 32% of the analysed particles in dry deposition and 65% in wet deposition. Category II (polymers grouped into chemically similar families) represented 31% and 20%, respectively, while Category III (indeterminate synthetic polymers) represented 37% of particles in dry samples and 15% of particles in wet samples.

Considering only the particles assigned to Category I, the overall distribution pattern was similar between dry- and wet-deposition samples, despite slight differences in relative abundances. Acryl (PMMA) was the dominant polymer in both conditions, accounting for 45% of identified particles in dry samples and 54% in wet samples (see Figure 14). In dry deposition, polyester (PES) was the second-most abundant polymer (25%), followed by polypropylene (PP) at 22%. In contrast, in wet-deposition samples, polypropylene (PP) ranked second (25%), while polyester (PES) ranked third (18%). Minor contributions from polymers were observed

in both sample types. In dry samples, polycarbonate (PC), polyethylene (PE), and polystyrene (PS) accounted for 4%, 3%, and 1%, respectively. In wet samples, lower proportions of polycarbonate (2%) and polyethylene (1%) were detected, while polystyrene was not observed.

In Category II, clear differences were observed between dry- and wet-deposition samples (see Figure 15). In dry-deposition samples, polyamide-type polymers were dominant, accounting for 45% of the particles in the group. Styrene-based polymers accounted for 19%, followed by polyester-type polymers at 16% and polyolefins at 12%. Minor contributions were observed for vinyl-based polymers (4%) and polyurethane-type polymers (4%). Nitrogen-containing and acrylic-type families were not detected in dry samples compared with wet samples. In contrast, wet-deposition samples exhibited a more distributed polymer profile. Polyester-type polymers were the most abundant group (32%), followed by polyamide-type polymers (27%) and styrene-based polymers (13%). Polyolefins remained relatively consistent (12%), while higher proportions of vinyl-based (7%) and polyurethane-type polymers (6%) were detected compared to dry deposition. Additionally, nitrogen-containing (2%) and acrylic-type polymers (1%) were identified exclusively in wet samples.

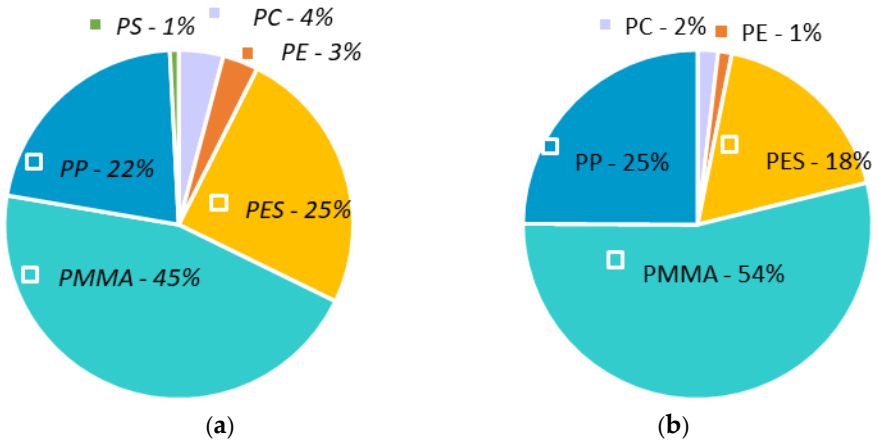

Figure 14. Relative distribution of unambiguously identified polymers (category I): (**a**) dry deposition; (**b**) wet deposition. PMMA: polymethyl methacrylate; PP: polypropylene; PES: polyester; PC: polycarbonate; PE: polyethylene; PS: polystyrene.

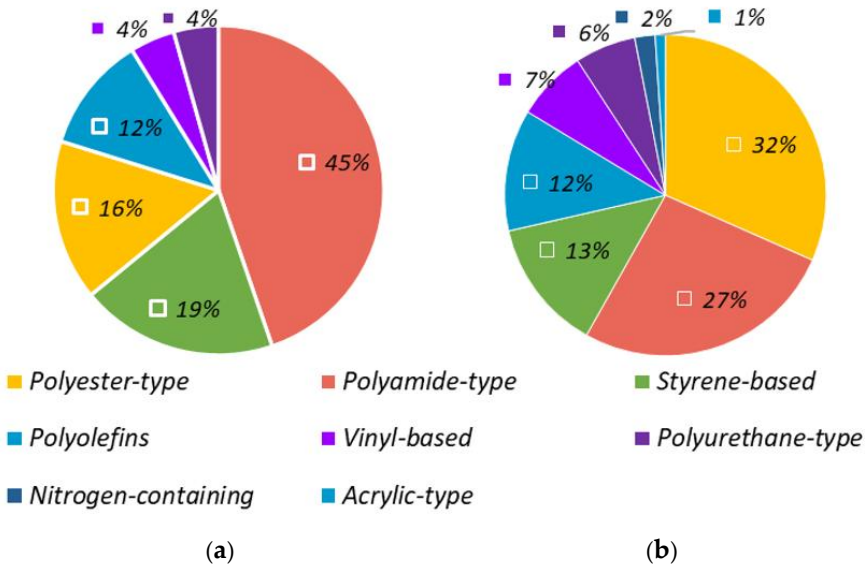

Figure 15. Relative distribution of polymers grouped into chemically similar families (category II): (**a**) dry deposition; (**b**) wet deposition.

Overall, while polyamide-type polymers dominated dry deposition, wet deposition showed a broader distribution of polymer families, with a relative enrichment of polyester-type and minor polymer groups.

In Category III, the proportion of particles whose Raman spectra exhibited signals corresponding to pigments was similar in dry and wet samples, at 43% and 39%, respectively. The remaining particles, suspected to be polymeric, could not be conclusively identified due to insufficient or ambiguous spectral information.

Across size fractions and spectra assigned to Category I, PMMA was the predominant polymer in wet deposition for both MPs and fibres (see Figure 16). Dry deposition showed greater variation, including PE dominance among MPs in the largest fraction and increased contributions of PES and PP in smaller fractions. Fibres showed a more consistent PMMA-dominated profile than MPs across both deposition modes.

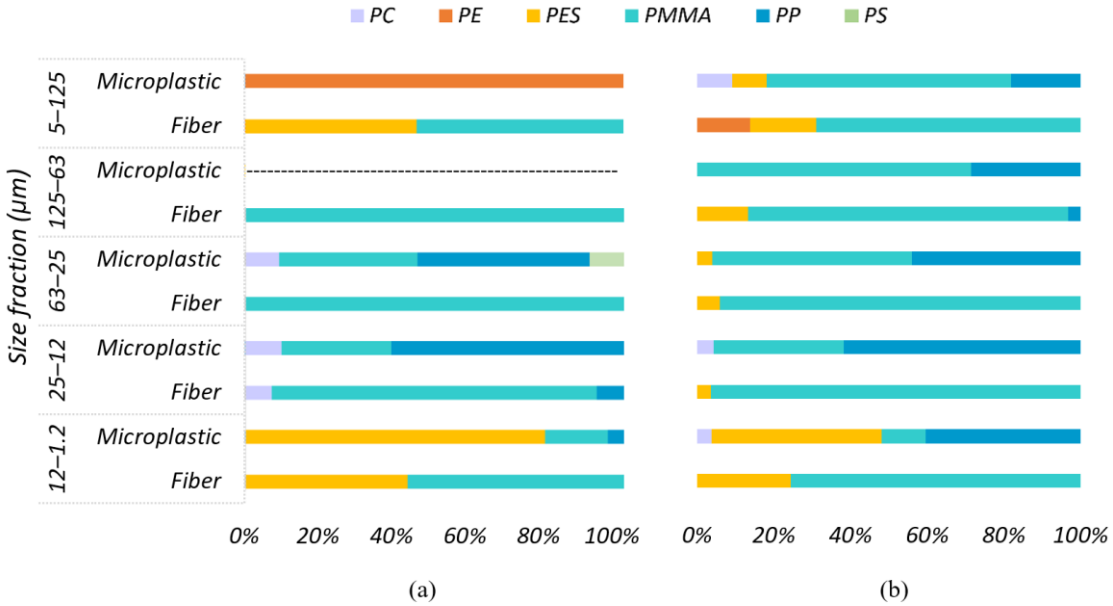

Figure 16. Relative distribution of unambiguously identified polymers (category I) in fractions: (**a**) dry deposition; (**b**) wet deposition. PMMA: polymethyl methacrylate; PP: polypropylene; PES: polyester; PC: polycarbonate; PE: polyethylene; PS: polystyrene.

Raman identification efficiency varied strongly with particle colour. Blue particles generally produced the highest proportion of interpretable spectra, with approximately 72% assigned to Category I. In contrast, transparent fibres showed poor Raman response: approximately 90% of all transparent fibres could not be identified due to the absence of clear spectral features, and only 11% were assigned to Category I. In comparison, 52% were classified as Category III and 35% as Category II. During the acquisition of spectra from weathered blue fibres, only the blue-coloured regions produced identifiable Raman signals. The transparent-white portions did not exhibit any detectable spectrum. At the same time, the transitional zone between blue and white-transparent showed only broad peaks, indicative of degradation. Still, without sufficient resolution to allow polymer identification (see Figure 17), orange and yellow particles also exhibited substantial spectral interference, with Category III accounting for approximately 83% and 69% of analysed particles, respectively, largely due to inorganic signals and fluorescence.

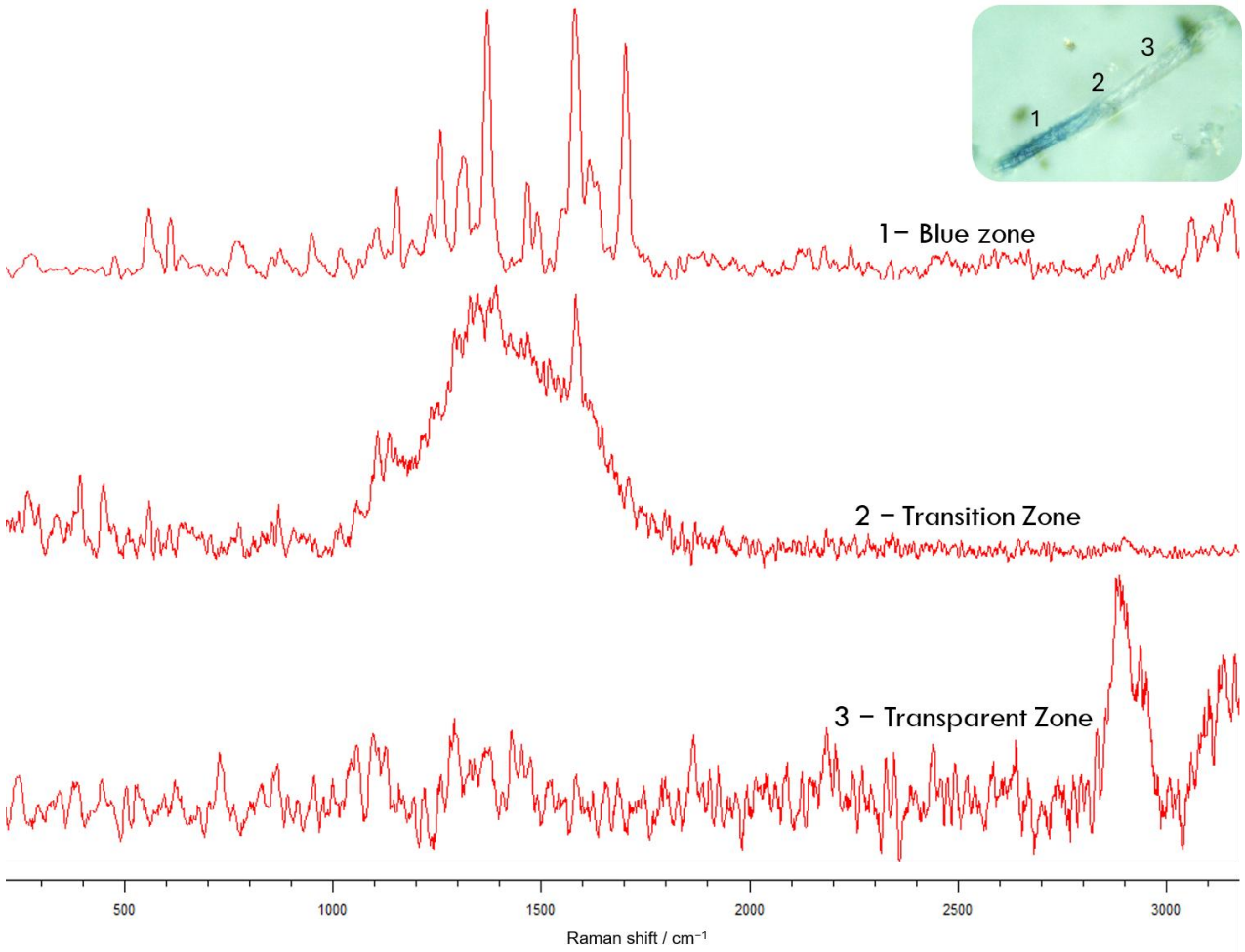

Figure 17. Raman spectra and microscope image of a partially degraded blue fibre showing spectral differences across zones (blue, transition and transparent zone).

3.5. Hierarchical Cluster Analysis of Raman Identification Profiles

HCA, based on the relative abundance of Category I polymers, separated the identified polymers into two main groups. PMMA and PES formed one cluster, while PP and PC formed another. PE and PS occurred as more distant branches, reflecting their restricted occurrence across the sampling events (Figure 18).

When Categories I–III were considered together, acrylic-, polyester- and polyolefin-type groups formed a cluster associated mainly with wet-deposition samples. In contrast, polyamide-type and indeterminate/other particles were more closely associated with dry-deposition samples (see Figure 18).

Clustering based on sample composition separated the three wet samples (B1–B3) from the three dry samples (A1–A3). Wet samples were characterised by higher relative contributions of acrylic and polyolefin groups and lower proportions of indeterminate particles, whereas dry samples showed higher proportions of indeterminate particles and polyamide- and styrene-based groups.

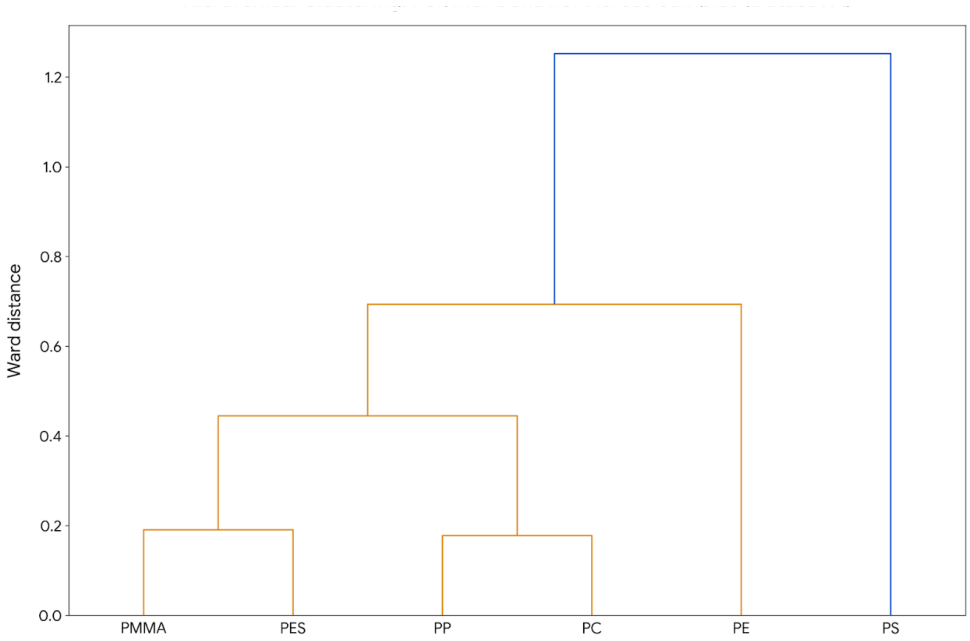

Figure 18. Hierarchical clustering analysis of category I (unambiguously identified polymers), based on the relative abundance of the identified polymers. PMMA: polymethyl methacrylate; PP: polypropylene; PES: polyester; PC: polycarbonate; PE: polyethylene; PS: polystyrene.

4. Discussion

The present study provides a detailed comparison of MPs and fibres in dry and wet deposition in the atmosphere and the removal of these particles in an urban environment under natural conditions. By combining size-fractionated sampling (ranging from 5 mm to 1.2 micrometres) with Raman-based polymer classification, the results reveal trend differences in MP and fibre particle abundance, spectral identification, and polymer distribution between dry and wet air deposition pathways and size fractions.

4.1. Dry and Wet Deposition of Atmospheric MPs and Fibres

The comparison between dry- and wet-deposition samples revealed differences in the atmospheric deposition rates of visually suspected MPs and identified fibres. Wet deposition showed mean rates of 3629 ± 449 MPs d^{-1} m^{-2} and 6515 ± 2683 fibres d^{-1} m^{-2}, compared with 427 ± 190 MPs d^{-1} m^{-2} and 2305 ± 829 fibres d^{-1} m^{-2} in dry deposition. Thus, the mean wet-deposition rates were approximately 8.5 times higher for MPs and 2.8 times higher for fibres. These differences are consistent with the role of precipitation in removing suspended particles from the atmosphere through wet scavenging processes (including below-cloud washout) and, potentially, in-cloud scavenging. The detection of large quantities of submicron particles in wet-deposition samples further reinforces this mechanism. Although these particles were below the Raman detection threshold, their abundance indicates that submicron-sized materials may represent a substantial yet underestimated fraction of atmospheric plastic contamination.

The deposition rates observed in the present study can also be considered in the context of previously reported atmospheric MP deposition measurements. However, direct quantitative comparisons between studies should be made with caution because of differences in sampling duration and strategies, collection devices, particle-size limits and ranges, and analytical identification criteria and methods. These methodological differences can substantially influence the reported deposition rates. For comparison, in Thailand, reported mean atmospheric MP deposition rates were 285 MPs m^{-2} day^{-1} for wet deposition and 199 MPs m^{-2} day^{-1} for dry deposition in a peri-urban area [7]. More recently, another study reported a mean number-based deposition rate of 881 MPs m^{-2} day^{-1}

at an urban site in Zurich, Switzerland, for particles in the 20–215 μm size range [27]. The values observed in the present study were higher, particularly for wet deposition (3629 MPs m^{-2} day^{-1}), whereas dry deposition averaged 427 MPs m^{-2} day^{-1}. Nevertheless, the present results contribute to the growing understanding of evidence that atmospheric MP deposition varies considerably across geographical locations and sampling conditions, highlighting the importance of harmonised sampling and analytical procedures.

The relative contribution of fibres also differed between deposition modes. In dry deposition, the visually identified fibre deposition was approximately five times higher than visually suspected MPs, whereas fibres were approximately 1.8 times more abundant in wet deposition. The greater visual variability observed among wet-deposition fibre samples suggests that fibre deposition may be particularly sensitive to the conditions prevailing during individual rainfall events. Such variability is consistent with the heterogeneous nature of atmospheric particle transport and deposition, as well as with the influence of meteorological conditions reported in previous atmospheric MPs studies [16,22].

Despite the pronounced difference in mean deposition rates, the exact Mann–Whitney U test did not indicate a statistically significant difference between deposition modes ($U = 0$, $p = 0.10$ for both MPs and fibres). This result should be interpreted in the context of the small number of independent sampling events ($n = 3$ per deposition mode). Therefore, the observed 8.5-fold and 2.8-fold differences provide descriptive evidence of contrasting deposition patterns.

An additional consideration is the difference in sampling duration between deposition modes. Dry-deposition samples represent cumulative particle collection over 8-day periods, whereas wet-deposition samples correspond to individual 24-hour rainfall events. Although deposition rates were normalised to a daily basis, these different collection periods may influence the comparability of the results. Furthermore, meteorological conditions during individual sampling events, including rainfall characteristics and atmospheric variability, may have contributed to the differences observed between samples. However, these parameters were not directly measured or recorded during the sampling campaigns, limiting the possibility of evaluating their individual influence on particle deposition. Therefore, the results should be interpreted as an exploratory comparison of the sampled deposition events.

The higher abundance of fine MPs and fibres observed in wet-deposition samples may indicate that precipitation is particularly effective at removing particles that remain suspended under dry conditions. However, the present sampling design does not allow the relative contributions of particle size, precipitation intensity, atmospheric residence time or other meteorological variables to be separated. Further sampling across a larger number of rainfall and dry-deposition events would therefore be required to establish the statistical robustness of these patterns.

4.2. Size Distribution, Morphology and the Effect of H_2O_2 Digestion

The distribution of visually suspected MPs and identified fibres across size fractions highlights the importance of considering particle morphology when interpreting atmospheric deposition. The structural properties of fibres—elongated shape, flexibility, and entanglement potential—can influence both atmospheric suspension and deposition dynamics [14,16,17]. Fibres showed greater variability in their distribution across size fractions during retention than compact fragments. Curling, entanglement, and aggregation can alter the effective dimensions of fibres and, therefore, their passage through sieve openings. Consequently, sieve-based size classification may not represent a simple measure of the physical length or width of individual fibres.

The contrasting distribution of fibres and MPs across size fractions also indicates that particle morphology should be considered when comparing deposition measurements. Fibres were generally more abundant than MPs in both deposition modes, but their relative distribution among fractions differed.

SEM observations of fraying, cracking and longitudinal splitting indicate morphological alteration of fibres and confirm their ongoing atmospheric degradation, [15,16] which may generate secondary MPs fragments and contribute to size redistribution across fractions, as for fibres and for MPs.

Oxidative digestion significantly affected the recovery of fine MPs. In wet deposition, 77% of MPs in the 25–12 μm and 52.0% in the 12–1.2 μm fraction were detected only after H_2O_2 treatment, whereas most MPs in the corresponding dry-deposition fraction were already detected before digestion (25–12 μm, 67.2%; 12–1.2 μm, 69.6%). This difference suggests that a substantial proportion of fine MPs in wet-deposition samples may be associated with organic or particulate matrices and therefore not readily accessible during direct filtration. The digestion step consequently provides an important methodological advantage by releasing particles that would otherwise remain undetected. The effect was less pronounced for fibres, for which most particles in the fine fractions were detected before digestion.

Although the increased recovery of fine particles following H_2O_2 treatment suggests that a proportion of these particles was initially associated with organic matter or larger particulate aggregates, the possibility of treatment-related effects should also be considered. The digestion procedure may modify the surrounding matrix and facilitate particle release; however, potential fragmentation of susceptible materials during oxidative treatment cannot be completely excluded.

This difference between MPs and fibres may reflect differences in particle geometry and in their interactions with the surrounding material. Overall, these findings demonstrate that sample-processing procedures can influence the apparent abundance and size distribution of atmospheric MPs and fibres and should therefore be considered when comparing deposition measurements among studies.

4.3. Raman Identification and Polymer Composition

The Raman analysis demonstrated that polymer identification was influenced by deposition mode and particle characteristics. Among the 1182 analysed spectra, 32% of dry-deposition particles and 65% of wet-deposition particles were assigned to Category I, corresponding to unambiguous polymer identification. Conversely, Category III accounted for 37% of dry-deposition particles but only 15% of wet-deposition particles. This difference indicates that the quality and interpretability of Raman spectra varied substantially between deposition conditions.

The higher proportion of indeterminate spectra in dry deposition could be consistent with greater spectral interference or surface alteration of the analysed particles. Atmospheric exposure may modify polymer surfaces through processes such as oxidation, mechanical abrasion and contamination. At the same time, pigments and additives may generate strong Raman signals or fluorescence that obscure polymer-specific bands. However, atmospheric residence time was not directly measured in the present study. Particle colour also influenced Raman identification. Blue particles generally produced more interpretable spectra, whereas transparent fibres were the most challenging group, with only a small proportion assigned to Category I (10%). Orange and yellow particles frequently produced spectra dominated by fluorescence or inorganic pigment signals. These observations demonstrate that visual colour alone cannot serve as an indicator of polymer identity and that pigment-related signals may interfere with the identification of the underlying polymer matrix.

PMMA, PES and PP dominated the polymer composition of Category I particles in both deposition modes. PMMA was particularly prominent among fibres, suggesting that this polymer represents an important component of the synthetic fibre fraction observed at the sampling site. However, polymer composition alone cannot be used to establish a specific source because the same polymer may originate from multiple products and emission pathways.

The size-dependent distribution of polymer types further indicates that the composition of atmospheric MPs is not uniform across particle fractions. The occurrence of different polymer groups among size classes may reflect differences in source material, particle fragmentation, atmospheric transport and deposition behaviour. The combined consideration of polymer identity, particle morphology and size therefore provides more information than polymer composition alone.

It should be noted that particle abundance was initially assessed through optical microscopy, while Raman spectroscopy was used to evaluate the chemical identity of a representative subset of the observed particles. Consequently, optical identification and spectroscopic confirmation represent different analytical levels.

Applying hierarchical clustering with Euclidean distance to normalised frequency matrices proved effective for this dataset. The hierarchical cluster analysis supported the distinction between deposition modes. When relative abundances of polymer families were considered, the three wet-deposition samples formed a common cluster. In contrast, the dry-deposition samples formed a separate branch, indicating that the differences between deposition modes are not subtle but instead represent primary drivers of variability within the dataset. Wet samples were characterised by relatively higher contributions of acrylic- and polyolefin-type polymers, whereas dry samples showed higher proportions of indeterminate and polyamide/styrene-based groups. Clustering by chemical family showed that Category II and Category III particles behave in environmentally consistent ways, grouping with their corresponding chemical families. Based on the hierarchical clustering results from multiple perspectives (sample type, polymer identification, and chemical family classification), the findings provide complementary confirmation of both the methodological approach and insight into the underlying environmental dynamics.

The presence of soot, rather than tyre resin, suggests that the observed black size particles are more likely derived from combustion processes than from traffic-related rubber abrasion. While tyre wear particles are a known source of airborne MPs, the analysed black and brown fragments did not originate from tyre materials.

The similar proportions of pigment-dominated spectra in both dry and wet samples (Category III) indicate that pigment persistence may exceed that of polymer backbone integrity during environmental ageing. This could suggest the presence of a degradation stage in which pigment structures remain spectroscopically stable even after partial alteration of the polymer matrix.

Transparent fibres exhibited the highest spectral ambiguity rate, reflecting both signal weakness and potential non-plastic composition. Transparent fibres posed the greatest analytical challenge: approximately 90% could not be identified because they lacked detectable Raman signals or were inorganic. These findings underline the importance of combining spectroscopic techniques with careful morphological assessment.

Furthermore, a "signal loss" effect was observed in weathered blue fibres. Weathered blue fibres showed polymer signals only in pigmented regions, while transparent portions often produced no detectable spectra. The similar proportion of pigment-dominated spectra in dry and wet samples may indicate that pigment-related Raman signals can remain detectable even when polymer-specific signals are weak or obscured. This possibility is supported by the observation of weathered blue fibres, for which Raman signals were retained mainly in pigmented regions.

The detection of high concentrations of bright unnaturally coloured submicron particles (≤0.5 μm)—estimated at ~109,000 in a single wet sample—highlights a significant but can be overlooked fraction of plastic pollution. Although submicron particles observed in wet-deposition samples could not be chemically confirmed because they were below the analytical size threshold of the Raman technique, and as extrapolated estimates were excluded from deposition rates calculated via optical microscopy quantification

(which relied on direct counts), their visual abundance suggests that many submicron-sized particles remain suspended in the atmosphere until their removal by rainfall.

The interaction between degradation processes, pigment persistence, and polymer identification suggests that atmospheric MPs may evolve through identifiable ageing stages. Understanding these stages is essential for improving classification accuracy and for interpreting atmospheric transport dynamics. Furthermore, the clear divergence between deposition mechanisms demonstrated in this study indicates that monitoring atmospheric microplastic pollution requires a comprehensive sampling strategy.

4.4. Integrated Methodological Implications and Limitations

The combined use of passive size-fractionated sampling, oxidative digestion, microscopy and Raman spectroscopy provided complementary information on atmospheric MPs and fibre deposition. Particle counting alone would not have captured the differences observed in morphology, size distribution, matrix association and polymer identification. In particular, the combination of size fractionation and H_2O_2 digestion demonstrated that the apparent abundance of fine MPs depends on sample-processing procedures. At the same time, Raman analysis revealed that chemical identification is strongly affected by particle colour and spectral quality.

The results also highlight important limitations of the analytical approach. Raman spectroscopy was not equally effective for all particle types, with transparent fibres, strongly pigmented particles and highly fluorescent particles presenting particular difficulties. Consequently, the absence of a positive polymer identification should not necessarily be interpreted as evidence that a particle is non-plastic. The Category III group should therefore be regarded as an analytical limitation rather than a chemically homogeneous particle class.

The observation of abundant submicron particles in wet deposition further underscores the need to extend atmospheric MPs investigations to smaller size ranges. However, because these particles were below the Raman analytical threshold used in this study, their polymeric nature could not be chemically confirmed. Future studies using analytical techniques capable of chemically characterising this size range would be required to establish their polymer composition.

Overall, the findings support an integrated approach in which deposition mode, particle morphology, size fraction and polymer composition are considered together. Such an approach can reduce the risk of underestimating atmospheric MP contamination from particles that are difficult to recover, classify, or chemically identify.

Despite the methodological advantages of the approach, several limitations should be considered when interpreting the findings. First, the limited number of independent sampling events (three per deposition mode) restricts statistical power and the generalisability of the observed differences. Second, the different sampling durations and potential meteorological variability may have influenced the deposition patterns. Third, Raman analysis was performed on selected subsets of the optically identified particles, with different proportions analysed for fragments, spheres and fibres. Consequently, the polymer composition identified by Raman spectroscopy may not fully represent that of all particles observed under optical microscopy. Furthermore, the identification success varied according to particle characteristics, particularly colour and morphology. These limitations should be considered when interpreting particle abundances and polymer composition and highlight the need for further investigations involving larger sampling datasets and complementary analytical techniques.

5. Conclusions

This study provided an integrated characterisation of visually suspected atmospheric MPs and atmospheric fibres in three dry- and three wet-deposition air collected samples

using size-fractionated passive sampling, microscopy, oxidative digestion and micro-Raman spectroscopy. The combined approach enabled evaluation of episodic deposition rates, particle morphology, size distribution, based on optical microscopy and consequent Raman polymer composition evaluation within a single analytical framework.

Wet deposition showed a higher mean of visually suspected MP deposition rates than dry deposition, with approximately 8.5-fold higher and 2.8-fold higher identified fibre deposition rates. However, the exact Mann–Whitney U test did not indicate statistically significant differences between deposition modes (U = 0, p = 0.10 for both MPs and fibres), and the small number of independent sampling events (n = 3 per deposition mode) limits the generalisability of the results. The observed differences should therefore be considered descriptive evidence of contrasting deposition patterns. Size fractionation demonstrated that MPs and fibres were not uniformly distributed across particle size classes, while oxidative digestion substantially increased the recovery of fine MPs, particularly in wet-deposition samples. These findings highlight the influence of particle–matrix interactions and sample-processing procedures on the apparent abundance and size distribution of atmospheric MPs.

A total of 1182 Raman spectra were acquired form particles selected through optical microscopy across all samples and size fractions. Polymer identification was more successful for wet-deposition samples, with 65% of particles assigned to Category I compared with 32% in dry deposition. PMMA, PES and PP were the dominant unambiguously identified polymers, while fluorescence, pigments, weak Raman signals and transparent fibres represented important limitations for chemical identification. Hierarchical cluster analysis further indicated distinct compositional profiles between dry- and wet-deposition samples.

Overall, the results demonstrate that atmospheric MP deposition cannot be fully characterised by particle abundance alone. Combining deposition mode, size fraction, morphology, sample processing and polymer identification provides a more comprehensive assessment of atmospheric MPs and fibres. It highlights methodological factors that may otherwise lead to underestimation. The detection of abundant submicron-sized particles also indicates the need for future studies using analytical approaches capable of chemically characterising particles below the Raman detection range.

Supplementary Materials: The following supporting information can be downloaded at https://www.mdpi.com/article/10.3390/environments13120646/s1, Table S1—Counts of microplastics and fibres from optical microscopy observation for dry- and wet-deposition samples, as for blank samples; Table S2—Dataset from Raman analysis of air particles (microplastics, fibres and spheres) including sample type, size-fraction, particle morphology and classification according to the study methodology. Table S3—Sample-level information on atmospheric deposition collection, including sample identification, collection dates, sampling duration, collector type, effective collection area, sampling height and GPS coordinates. Figure S1—Schematic workflow of sample size fractionation, direct filtration and H_2O_2-assisted particle recovery. Material retained on the 125, 63 and 25 μm meshes was subjected to oxidative digestion (15% H_2O_2, 50 °C, 12 h), followed by refiltration. Fine particles recovered through direct filtration and after digestion 25–12 μm and 12–1.2 μm were counted separately, with post-digestion counts representing additional particle recovery without duplication. Figure S2—Representative Raman spectrum of an example of styrene-based polymer based on characteristic pick—assigned to Category II. Figure S3—Representative processed Raman spectrum of a particle classified as Category III (indeterminate synthetic polymer). Despite spectral processing, the spectrum did not provide sufficient diagnostic evidence to assign the particle to an individual polymer or a chemically similar polymer family. Figure S4—Example of a Raman spectrum classified as Category III, in which the available spectral features were insufficient for reliable identification of a polymer or polymer family.

Author Contributions: Conceptualization, Y.L., H.R., L.P.d.S. and J.E.d.S.; methodology, Y.L., H.R., L.P.d.S. and J.E.d.S.; validation, Y.L.; formal analysis, Y.L. and R.V.; investigation, Y.L., H.R. and

L.P.d.S.; data curation, Y.L.; writing—original draft preparation, Y.L., H.R., J.E.d.S.; writing—review and editing, J.A.M., H.R., L.P.d.S. and J.E.d.S.; visualization, Y.L., H.R. and J.E.d.S.; supervision, H.R., L.P.d.S. and J.E.d.S.; funding acquisition, H.R., L.P.d.S. and J.E.d.S. All authors have read and agreed to the published version of the manuscript.

Funding: This research received no external funding.

Institutional Review Board Statement: Not applicable.

Informed Consent Statement: Not applicable.

Data Availability Statement: The data presented in this study are available on request from the corresponding author.

Acknowledgments: The Portuguese "Fundação para a Ciência e Tecnologia" (FCT, Lisbon) is acknowledged for funding the project PTDC/QUI-QFI/2870/2020 as well as the R&D Unit CIQUP (UIDB/00081/2020 and UIDP/00081/2020), the R&D Unit IFIMUP (UID/4968/2025) and the Associated Laboratory IMS (LA/P/0056/2020). FCT is acknowledged for funding the PhD grant of Yuliya Logvina (2022.14123.BD), and Luís Pinto da Silva acknowledges funding from FCT under the Scientific Employment Stimulus (CEECINST/00069/2021). The authors acknowledge the Functional Centres of the University of Porto (CEMUP), especially Rui Rocha, for providing SEM analysis and technical support.

Conflicts of Interest: The authors declare no conflicts of interest.

Abbreviations

The following abbreviations are used in this manuscript:

MPs	Microplastics
PA	Polyamide
PE	Polyethylene
PES	Polyester
PET	Polyethylene terephthalate
PMMA	Polymethyl methacrylate
PP	Polypropylene
PS	Polystyrene

References

1. Thompson, R.C.; Olsen, Y.; Mitchell, R.P.; Davis, A.; Rowland, S.J.; John, A.W.G.; McGonigle, D.; Russell, A.E. Lost at Sea: Where Is All the Plastic? *Science* **2004**, *304*, 838. https://doi.org/10.1126/science.1094559.
2. Tan, Y.; Dai, J.; Xiao, S.; Tang, Z.; Zhang, J.; Wu, S.; Wu, X.; Deng, Y. Occurrence of Microplastic Pollution in Rivers Globally: Driving Factors of Distribution and Ecological Risk Assessment. *Sci. Total Environ.* **2023**, *904*, 165979. https://doi.org/10.1016/j.scitotenv.2023.165979.
3. Lebreton, L.C.M.; van der Zwet, J.; Damsteeg, J.-W.; Slat, B.; Andrady, A.; Reisser, J. River Plastic Emissions to the World's Oceans. *Nat. Commun.* **2017**, *8*, 15611. https://doi.org/10.1038/ncomms15611.
4. Singh, B.P. Understanding the Dynamics and Implications of Airborne Microplastics in Atmosphere. *Air Qual. Atmos. Health* **2024**, *17*, 2661–2674. https://doi.org/10.1007/s11869-024-01593-4.
5. Zhang, N.; Zhang, C.; Qin, Y.; Wang, J.; Ge, X.; Li, H.; Dai, Y.; Aruffo, E. A Review of Atmospheric Microplastics: Sources, Characteristics, and Detection Method. *Curr. Pollut. Rep.* **2024**, *10*, 412–429. https://doi.org/10.1007/s40726-024-00316-8.
6. Liu, Y.; Nie, Z.; Meng, Y.; Liu, G.; Chen, Y.; Chai, G. Influence of Meteorological Conditions on Atmospheric Microplastic Transport and Deposition. *Environ. Res.* **2025**, *265*, 120460. https://doi.org/10.1016/j.envres.2024.120460.
7. Winijkul, E.; Latt, K.Z.; Limsiriwong, K.; Pussayanavin, T.; Prapaspongsa, T. Depositions of Airborne Microplastics during the Wet and Dry Seasons in Pathum Thani, Thailand. *Atmos. Pollut. Res.* **2024**, *15*, 102242. https://doi.org/10.1016/j.apr.2024.102242.
8. Cai, Y.; Yang, T.; Mitrano, D.M.; Heuberger, M.; Hufenus, R.; Nowack, B. Systematic Study of Microplastic Fiber Release from 12 Different Polyester Textiles during Washing. *Environ. Sci. Technol.* **2020**, *54*, 4847–4855. https://doi.org/10.1021/acs.est.9b07395.

9. Park, I.; Lee, J.; Lee, S. Laboratory Study of the Generation of Nanoparticles from Tire Tread. *Aerosol Sci. Technol.* **2017**, *51*, 188–197. https://doi.org/10.1080/02786826.2016.1248757.
10. Vallabani, N.V.S.; Gruzieva, O.; Elihn, K.; Juárez-Facio, A.T.; Steimer, S.S.; Kuhn, J.; Silvergren, S.; Portugal, J.; Piña, B.; Olofsson, U.; et al. Toxicity and Health Effects of Ultrafine Particles: Towards an Understanding of the Relative Impacts of Different Transport Modes. *Environ. Res.* **2023**, *231*, 116186. https://doi.org/10.1016/j.envres.2023.116186.
11. Kole, P.J.; Löhr, A.J.; Belleghem, F.G.A.J.V.; Ragas, A.M.J. Wear and Tear of Tyres: A Stealthy Source of Microplastics in the Environment. *Int. J. Environ. Res. Public Health* **2017**, *14*, 1265. https://doi.org/10.3390/ijerph14101265.
12. Luo, Z.; Zhou, X.; Su, Y.; Wang, H.; Yu, R.; Zhou, S.; Xu, E.G.; Xing, B. Environmental Occurrence, Fate, Impact, and Potential Solution of Tire Microplastics: Similarities and Differences with Tire Wear Particles. *Sci. Total Environ.* **2021**, *795*, 148902. https://doi.org/10.1016/j.scitotenv.2021.148902.
13. Singh, P.; Singh, Y.; Paleologos, E.K.; Banasiak, L.; O'Kelly, B.C.; Bokade, M.; Mohamed, A.-M.O.; Hursthouse, A.; Sarris, T.; Singh, D.N. A Review of Rubber Tyre Derived Micro- and Nanoplastics: Fate, Impact and Risks. *Environ. Geotech.* **2025**, *12*, 691–708. https://doi.org/10.1680/jenge.24.00159.
14. Xiao, S.; Cui, Y.; Brahney, J.; Mahowald, N.M.; Li, Q. Long-Distance Atmospheric Transport of Microplastic Fibres Influenced by Their Shapes. *Nat. Geosci.* **2023**, *16*, 863–870. https://doi.org/10.1038/s41561-023-01264-6.
15. Mossotti, R.; Dalla Fontana, G.; Anceschi, A.; Gasparin, E.; Battistini, T. Preparation and Analysis of Standards Containing Microfilaments/Microplastic with Fibre Shape. *Chemosphere* **2021**, *270*, 129410. https://doi.org/10.1016/j.chemosphere.2020.129410.
16. Tatsii, D.; Bucci, S.; Bhowmick, T.; Guettler, J.; Bakels, L.; Bagheri, G.; Stohl, A. Shape Matters: Long-Range Transport of Microplastic Fibers in the Atmosphere. *Environ. Sci. Technol.* **2024**, *58*, 671–682. https://doi.org/10.1021/acs.est.3c08209.
17. Kärkkäinen, N.; Sillanpää, M. Quantification of Different Microplastic Fibres Discharged from Textiles in Machine Wash and Tumble Drying. *Environ. Sci. Pollut. Res.* **2021**, *28*, 16253–16263. https://doi.org/10.1007/s11356-020-11988-2.
18. Sharma, P.; Sharma, P.; Abhishek, K. Sampling, Separation, and Characterization Methodology for Quantification of Microplastic from the Environment. *J. Hazard. Mater. Adv.* **2024**, *14*, 100416. https://doi.org/10.1016/j.hazadv.2024.100416.
19. Logvina, Y.; Matas, I.M.; Ribeiro, H.; Pinto da Silva, L.; Rodrigues, P.; Leitão, J.; da Silva, J.E. Micro- and Nanoplastics in the Atmosphere: Methodology for Microplastics Size-Fractionation Sampling. *Microplastics* **2024**, *3*, 82–97. https://doi.org/10.3390/microplastics3010006.
20. Markovic, M.Z.; Prokop, S.; Staebler, R.M.; Liggio, J.; Harner, T. Evaluation of the Particle Infiltration Efficiency of Three Passive Samplers and the PS-1 Active Air Sampler. *Atmos. Environ.* **2015**, *112*, 289–293. https://doi.org/10.1016/j.atmosenv.2015.04.051.
21. Munno, K.; De Frond, H.; O'Donnell, B.; Rochman, C.M. Increasing the Accessibility for Characterizing Microplastics: Introducing New Application-Based and Spectral Libraries of Plastic Particles (SLoPP and SLoPP-E). *Anal. Chem.* **2020**, *92*, 2443–2451. https://doi.org/10.1021/acs.analchem.9b03626.
22. Logvina, Y.; Moreira, D.S.; Santos, R.P.M.; Neves, I.F.; Ribeiro, H.; Pinto da Silva, L.; Esteves da Silva, J. Microplastic Aerosol Contamination in Porto (Portugal). *Microplastics* **2024**, *3*, 696–716. https://doi.org/10.3390/microplastics3040043.
23. ISO/DIS 4222.2; Air quality—Measurement of atmospheric dustfall – Horizontal deposit gauge method. International Organization for Standardization: Geneva, Switzerland, 1980.
24. Cowger, W.; Gray, A.; Christiansen, S.H.; DeFrond, H.; Deshpande, A.D.; Hemabessiere, L.; Lee, E.; Mill, L.; Munno, K.; Ossmann, B.E.; et al. Critical Review of Processing and Classification Techniques for Images and Spectra in Microplastic Research. *Appl. Spectrosc.* **2020**, *74*, 989–1010. https://doi.org/10.1177/0003702820929064.
25. CHSOS. Available online: https://chsopensource.org/ (accessed on 4 March 2026).
26. Chen, L.; Cao, Y.; Hu, X.; Zhang, B.; Chen, X.; Cui, B.; Xu, J.; Yu, T.; Xu, Z. Raman Spectral Optimization for Soot Particles: A Comparative Analysis of Fitting Models and Machine Learning Enhanced Characterization in Combustion Systems. *Build. Environ.* **2025**, *271*, 112600. https://doi.org/10.1016/j.buildenv.2025.112600.
27. Ashta, N.M.; Crosset-Perrotin, G.; Moraz, A.; Philipp, M.; Bucheli, T.D.; Kaegi, R.; Hueglin, C. Wet and Dry Atmospheric Deposition of Microplastics at Urban, Suburban, Rural and Mountainous Sites in Switzerland. *Atmos. Chem. Phys.* **2026**, *26*, 11803–11815. https://doi.org/10.5194/acp-26-11803-2026.

Disclaimer/Publisher's Note: The statements, opinions and data contained in all publications are solely those of the individual author(s) and contributor(s) and not of MDPI and/or the editor(s). MDPI and/or the editor(s) disclaim responsibility for any injury to people or property resulting from any ideas, methods, instructions or products referred to in the content.